Advanced Steel Construction – Vol. 15 No. 1 (2019) 47–54
DOI:10.18057/IJASC.2019.15.1.7

BEHAVIOR OF CFST-COLUMN TO STEEL-BEAM JOINTS IN THE SCENARIO OF COLUMN LOSS

Shan Gao[1,2], Man Xu[3,*], Lan-Hui Guo[4] and Su-Mei Zhang[4]

[1] *Shaanxi Key Laboratory of safety and durability of concrete structures, Xijing University, Xian 710000, China*
[2] *Postdoctoral Station of Civil Engineering, Chongqing University, Chongqing 400030, China*
[3] *School of Civil Engineering, Northeast Forestry University, Harbin 150090, China*
[4] *School of Civil Engineering, Harbin Institute of Technology, Harbin 150090, China*
** (E-mail: xuman@nefu.edu.cn)*

ABSTRACT

As a connecting component in structures, the mechanical property of joint is one of the critical factors, especially to prevent progressive collapse. In the scenario of column loss, the joints are subjected to bending moment combined with tension to redistribute loads, which is different from the behavior of joint in an undamaged structure. According to this specific loading condition, two concrete-filled steel tubular column-steel beam joints under bending moment combined with tensile force were tested. In the test, a new kind of semi-rigid joint was proposed, whilst an outer-ring configuration was adopted in a rigid joint for comparison. Meanwhile a finite element model of the new joint was developed by using ABAQUS. The results show that new semi-rigid joint possesses good rotation capacity under pure bending moment. The initial stiffness and moment resistance of the new joint are both smaller than those of the outer-ring joint. The moment-tension relationship of new joint keeps linear. The behavior of joint under moment combined with tensile force may be uniformly described by a power function correlation expression. The influence of width of short-limb connected to tube wall and the limb thickness on the initial stiffness and strength of new joint is obvious whilst the influence of width of long-limb connected to beam flange is not evident.

ARTICLE HISTORY

Received: 15 April 2017
Revised: 18 December 2017
Accepted: 27 December 2017

KEYWORDS

concrete-filled steel tubular;
progressive collapse;
bending moment combined with tension;
semi-rigid;
beam-column joint

1. Introduction

Progressive collapse in high-rise building structures will result in significant casualties and property loss. The partial collapse of Ronan Point apartment is deemed as a milestone of structural progressive collapse. The notorious terrorism attack of World Trade Center in 2001 triggered more interests on the progressive collapse resistance of building structures. As a connecting component of structural members, the mechanical property of joint is one of the critical factors, especially to prevent progressive collapse.

Once an internal column is damaged and loses its load-carrying capacity, vertical loads would seek another load path to distribute and normally are sustained by the beams connected to the damaged column. The vertical loads would cause large deflection of two-span beam and require the above joint to bridge over the damaged column. The load-carrying mechanism of the joint would transfer from lumped plastic hinge action to catenary action. In this condition, the joint should bear additional tensile force besides moment to transfer the vertical loads to the remaining structure, after tensile catenary action is triggered at the beams. Meanwhile, the joints would undergo large deformation without any significant reduction in strength. During the transition of load-carrying mechanism, the joints at the damaged column and the adjacent columns should be capable of carrying reverse bending moments and additional tensile forces at the same time. The increasing tensile force would influence the bending resistance of the joint. There features are seldom to encounter in conventional design but essential for preventing progressive collapse in structure under column loss. It is crucial to study the performance of the joint in this transition of load-carrying mechanism.

Alternative Load Path method is widely adopted in various national codes and standards (BS [1], GSA [2], DoD [3]) to analyze progressive collapse resistance of structures. Redundancy and ductility of joints are required specifically in Alternative Load Path method, in order to dissipate energy and avoid brittle damage of joint. In addition to moment resistance and initial stiffness, the ability of load-carrying mechanism transformation of joints is more concerned. The joints should undergo tensile loads without any significant reduction in strength and rotation capacity. Large deformation in the damaged part of structure is allowed, as long as progressive collapse is prevented (Haremza et al. [4]). Compared with rigid connection, semi-rigid connection can optimize the bending moment distribution in the connected beams. More importantly, compared with rigid joints, semi-rigid joints possess better rotation capacity which is beneficial for activating "catenary action" in the system of preventing progressive collapse.

So far, many numerical and analytical studies have been carried out on the behavior of whole structure and the joint in the scenario of internal column removal (Buscemi et al. [5], Gerasimidis et al. [6], Izzuddin et al. [7], Iribarren et al. [8], Khandelwal et al. [9], Li et al. [10], Stylianidis et al. [11], Xu et al. [12], Yu et al. [13]). A significant development of theory, mechanical model and design method about progressive collapse have been proposed. However, more convincing experiments still need to be performed. Yi et al. [14] tested a 1/3-scaled 3-story RC frame with 4 bays in the scenario of middle column loss. The results showed that the RC frame under middle column loss would undergo 4 stages including elastic stage, elastic-plastic stage, plastic stage and catenary stage. Demonceau et al. [15] conducted a static test of a steel frame with RC floor slab in the scenario of internal column removal. Flush endplate beam-column connections were adopted in the steel frame. The registered curves confirmed the development of tying force in the beams. Sadek et al. [16] tested various steel joints and RC joints in the scenario of progressive collapse. Portions of structural framing systems were designed as the boundary condition of the joints. The experimental results presented the behavior and failure modes of steel joints and RC joints. Li and Wang et al. [17] conducted two full-scale tests on steel beam-to-tubular column moment connections with outer-diaphragm under a column removal scenario. Two types of flexural failure modes, namely a continuous flexural failure throughout the section and an interrupted flexural failure without the fracture extending upwards were observed from the tests. Yang et al. [18] conducted an experimental test to estimate the progressive collapse resistance of composite frame under a middle column loss. The experimental results indicated that more reinforcing bars should be used in composite slab and the effectiveness of the enhanced tie forces was investigated. Qian et al. [19] proposed a simple approach which can be used to evaluate the progressive collapse vulnerability of RC buildings under multiple column removal scenarios. Guo and Gao et al. [20-21] performed a series of research project to investigate the behavior of steel structure with RC slab under an internal column-removal scenario. This research work involved a series of tests on steel frame and steel joints with RC slab, finite element study of joint and structure behavior, and development of mechanical models.

Previous studies have been attracted into steel structures and reinforced concrete structures, few attentions are paid on composite structures. In this paper, experimental study and theoretical analysis had been performed on the moment-tension performance of concrete-filled steel tubular (CFST) column to steel-beam joints. A new type of semi-rigid connection was proposed and studied in detail. In addition, parametric analysis on the behavior of the new joint was also conducted by ABAQUS. The influence of angle on the behavior of new joint was analyzed.

2. Experimental program

2.1. Design and fabrication of specimen

According to the experimental set-up, two 1/3-scale specimens of CFST-column to steel-beam joints were designed and fabricated. Outer-ring connection was adopted as rigid joint whilst a new type connection was applied as semi-rigid joint, which can be easily assembled.

The dimension of the rigid joint is shown in Fig. 1. The width and thickness of square steel tube used in CFST column were 160 mm and 5 mm respectively. The profile section of steel beam was H200×100×5.5×8 [H-overall depth×flange width×web thickness×flange thickness]. Two outer-ring plates and a shear plate were welded to the wall of square tube by using fillet weld. The thickness of outer ring plate and shear plate was both 10mm. The flanges of steel beam were welded to the outer-ring plate whilst the web of steel beam was welded to a shear plate on the column. Connection plates which were used to apply tensile forces were welded to the ends of steel beams. A pair of stiffeners was welded to steel beam at the position of hinge support.

Normally, rigid joints such as outer-ring and inner-ring connection are usually adopted in practical buildings with CFST columns. Due to the relatively complicated configuration, semi-rigid joints are not widely used in public building structures, even though semi-rigid joints can optimize the bending moment distribution in the connected beams. As aforementioned, it is also especially beneficial for the system of preventing progressive collapse.

As typical semi-rigid joint, end-plates joints are usually adopted to connect steel-beam to the rectangular section columns. The solutions shown in Fig. 2(a) (Hoang [22]) are usually adopted in the construction, namely use of special bolts or use of intermediate elements. These solutions are adopted to overcome the difficulty of placing bolts in the closed column section. However, the two above joint solutions have some disadvantages in their cost and their generally low bending stiffness and resistance. Meanwhile the mechanical behavior of the mentioned joint is mainly governed by the bolts, which presents generally a rather weak ductility under tensile force. Accordingly, the above joint solutions are normally not suitable to be used for moment resistant frames in seismic and anti-collapse design.

The new joint is shown in Fig. 2(b). Unequal limb angles were employed to accompany this semi-rigid connection. Four short-limbs could circle a close hoop to ensure the effective transformation of loads from beams to column. The new joint could be easily assembled in construction site by welding seams and bolts. Short-limb of angle and shear plate were welded to square steel tube. Meanwhile a stiffener was welded in the middle of the angle to improve the stiffness of the connection. Then the flanges of steel beam were connected to long-limb by high-strength bolts whilst the web of steel beam was connected to a shear plate on tube wall by the same way. The same configuration was adopted in both top flange and bottom flange of steel beam.

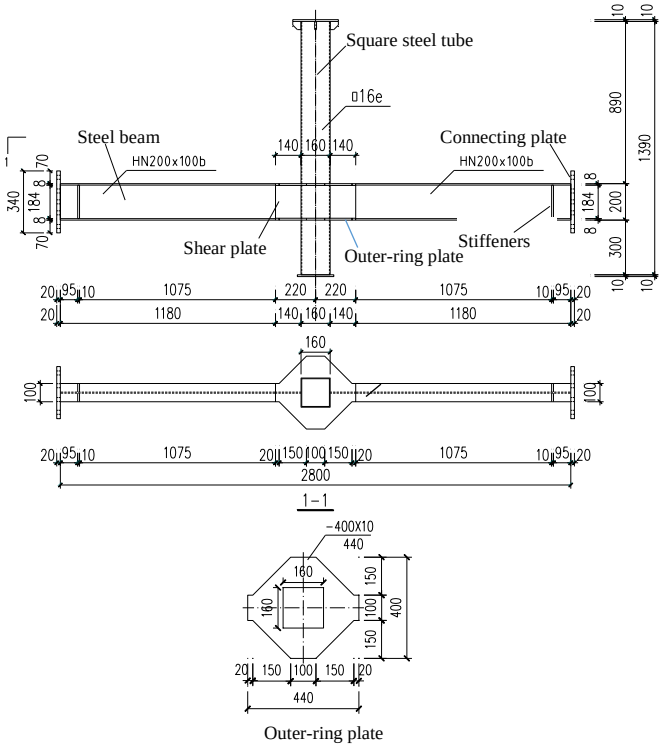

Fig. 1 Dimension of specimens for rigid outer-ring connection (SJ01)

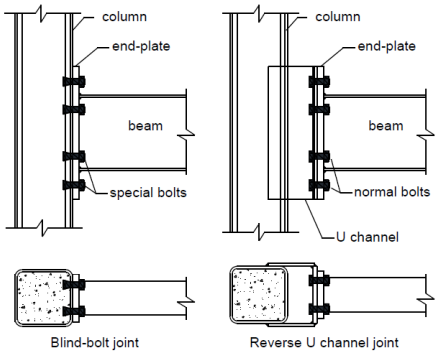

(a) Blind-bolt and reverse U channel joints (Hoang [22])

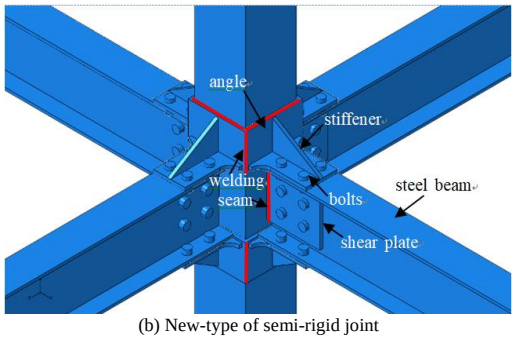

(b) New-type of semi-rigid joint

Fig. 2 Steel beam-CFST column joints

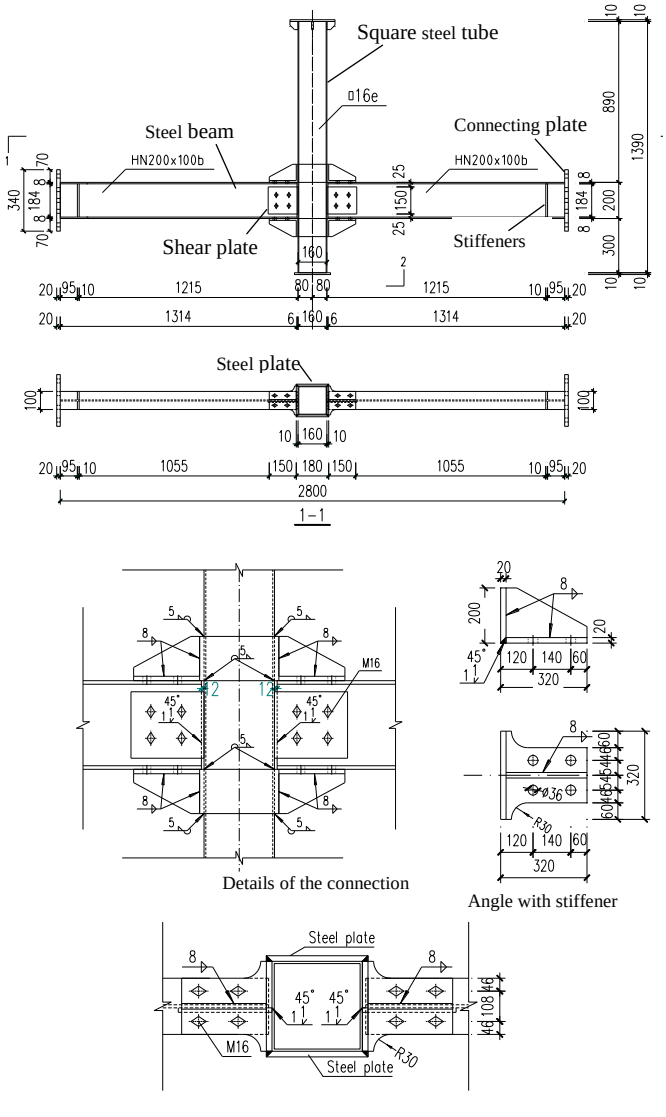

Fig. 3 Dimension of specimens for semi-rigid connections (SJ02)

The dimension of the semi-rigid joints (SJ02) is shown in Fig. 3. Only in-plane connection was designed. To this end, 10 mm steel plates were used to connect the angle on both sides of the joint. The dimensions of square steel tube and steel beam used in specimen SJ02 were identical with SJ01. The thickness of stiffener and shear plate was 10mm. The cross section of angle was ∟160 ×100×10 [∟-Long limb width×Short limb width×Limb thickness]. M16 high-strength bolts with grade 10.9 were used in the connections.

2.2. Material properties

In the test, Chinese grade Q235B structural steel was used for all steel members. Standard coupons were cut from each steel member and tested. The material properties of steel are listed in Table 1, where f_y, f_u, E_s are steel yield strength, tensile strength and elastic modulus respectively. Casting of 150×150×150 mm cubes for concrete strength test and 150×150×300 mm cylinder for concrete Young's modulus were carried out at the same time. They were cured in similar conditions as the specimen. The average compressive strength of concrete cubes is 33.1 MPa. The Young's modulus of concrete is 2.29×10^4MPa.

Table 1
Mechanical properties of steel

Se.		*t* (mm)	f_y (MPa)	f_u (MPa)	E_s (10^5MPa)
Beam	Flange	7.1	269	401	1.96
	Web	5.2	275	411	2.09
Square tube		4.8	342	402	1.82
Ring plate/Shear plate		9.2	298	388	1.91

2.3. Loading procedure

In the scenario of column loss, the joint would be under the load combination of bending moment and tensile force during the transition of load-carrying mechanism. Hence the load combination was applied onto the specimens through two steps as shown in Fig. 4:

Step A: Apply vertical load on the column. Through applying vertical load, a bending moment is applied on the joint. After the plastic yield moment of the joint is reached, the vertical jack would be arrested and hold constantly. The beam-ends rotate freely while the vertical load is applied in order to avoid additional tensile force occurring in the beams.

Step B: Apply horizontal tensile force at both ends of the beams. While the rotation of the joint is kept a constant value, the ends of the beams are continuously loaded until the joint fails.

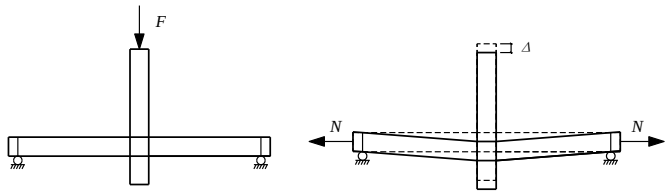

(a) Step A (b) Step B

Fig. 4 Loading steps

2.4. Experimental setup

The specimens were tested in the multifunctional loading ring as shown in Fig. 5 (see Guo and Gao et al. [21] for more details). With this loading ring, moment and tensile force could be applied to the joints simultaneously. The details of the experimental setup are illustrated in Fig. 6.

In loading step A, the beam-ends should rotate freely while the vertical load was applied through hydraulic jack (3), in order to avoid additional tensional force occurring in the beam. As shown in Fig. 6, the bottom flange of steel beam where was strengthened by a pair of stiffeners was placed on hinge support (10) to realize boundary condition of simple support. The beam-end was connected to the connecting hinge (9) by high-strength bolts, while the connecting hinge (9) was connected with bolt sleeve (8) by a pivot shaft. This connecting unit could make beam-ends rotate freely while the vertical load was applied. In loading step B, tension rod (7) was screwed into bolt sleeve (8) to transfer the tensile load applied by horizontal jack to the specimen.

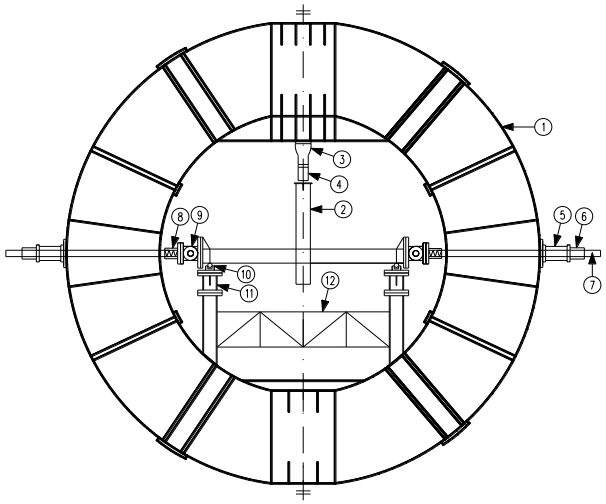

Fig. 5 Experimental setup:

(1) multifunctional loading ring; (2) specimen; (3) 500kN hydraulic jack; (4) load cell;(5) 2500kN hydraulic jack; (6) load cell; (7) 90mm-diameter tension rod; (8) bolt sleeve; (9) connecting hinge; (10) hinge support; (11) support column; (12) column bracing

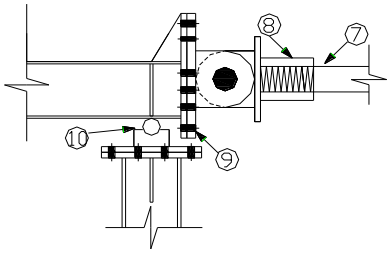

Fig. 6 Hinge support

Linear variable displacement transducers (LVDT) were placed to monitor the displacements of the specimens. The distribution of LVDTs is presented in Fig. 7. The following values were measured: vertical displacement of column (LVDT 1) and beams (LVDT 8-LVDT 9); axial deformation of steel beams (LVDT 2-LVDT 3); horizontal displacement of column (LVDT 4-LVDT 5); support settlement (LVDT 6-LVDT 7). Uniaxial and rosette strain gauges were arranged on the specimen, as shown in Fig. 8.

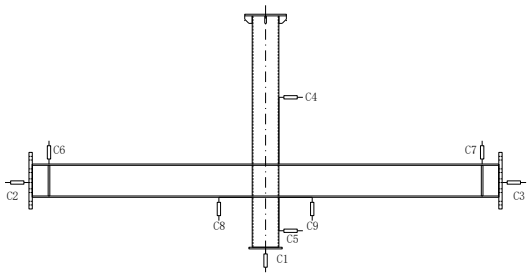

Fig. 7 Distribution of LVDTs

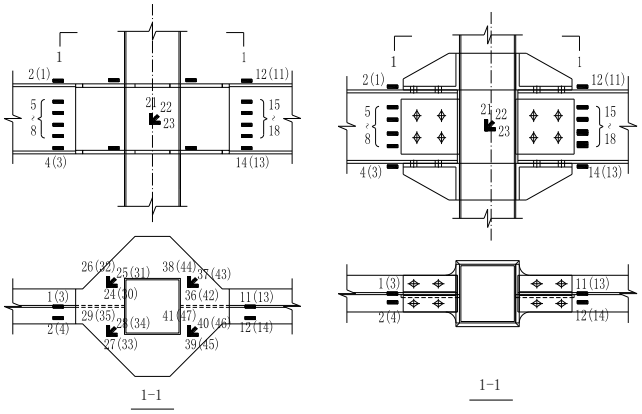

(a) SJ01 (b) SJ02

Fig. 8 Distribution of strain gauges

3. Experimental phenomena

3.1. Specimen SJ01

Before the yield load reached, no evident phenomenon was observed in step A. At the end of loading step A, the vertical displacement of specimen SJ01 was only 10 mm. And then horizontal tensile load was applied onto both ends of the beams whereas the vertical load was 80 kN. With the increase of tensile loads, several cracks were appeared on the oxide scale of steel beam. Loading was terminated when the horizontal displacement of steel-beam increased remarkably. Besides the bending deformation of the steel beam, no other phenomenon, such as severe local buckling or fracture, was occurred on the specimen SJ01, as shown in Fig. 9.

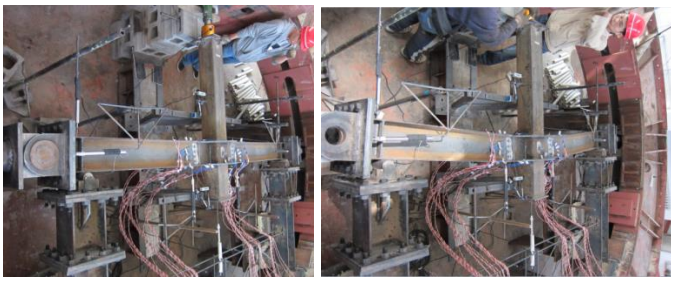

(a) Before loading (d) After loading

Fig. 9 Phenomena of specimen SJ01

3.2. Specimen SJ02

No evident phenomenon was observed in the joint in loading step A. At the end of loading step A, the vertical load on specimen SJ02 was 60 kN and the corresponding vertical displacement was 12 mm. And then, horizontal tensile load was applied on both ends of steel beams. When the tensile load increased to 480 kN, the tube wall deformed remarkably as shown in Fig. 10(b). With the increase of tensile load, the deformation of tube wall gradually increased. At 625 kN, the loading was terminated due to the fracture of the welding seams between angle and steel plate at the right-side connection as shown in Fig. 10(c-d).

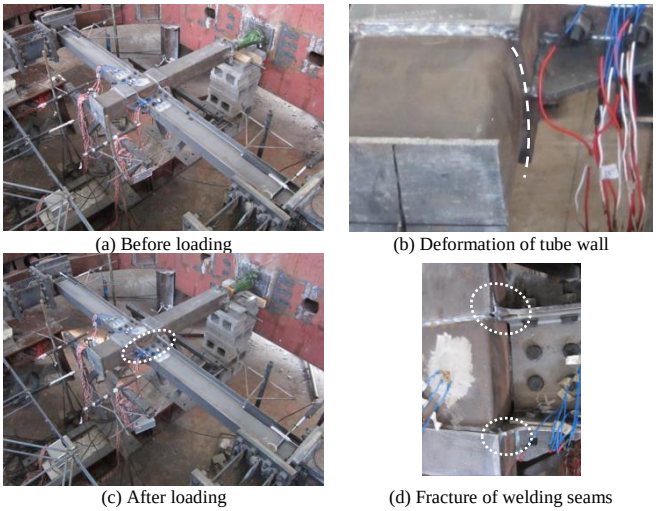

(a) Before loading (b) Deformation of tube wall

(c) After loading (d) Fracture of welding seams

Fig. 10 Phenomena of specimen SJ02

4. Experimental results and discussions

4.1. Relationship between bending moment and tensile force

Fig. 11(a) shows the bending moment-rotation angle curves of specimen SJ01 and specimen SJ02 in loading step A. The bending moment of joints is calculated by using the following expression:

$$M = P/2 \cdot L \tag{1}$$

where P stands for the vertical load applied at the top of column ; L for the length of beam which is 1.05 m; M for the bending moment.

The rotation angle of the specimens is given as follows:

$$\theta = \Delta / L \tag{2}$$

$$\Delta = u_m - \frac{1}{2}\left(u_l + u_r\right) \tag{3}$$

where Δ stands for the vertical displacement of column; u_{m} for the vertical displacement of column directly obtained from LVDT 1 shown in Fig. 7; u_{l} and u_{r} for the left support deformation and right support deformation obtained from LVDT 6 and LVDT 7 respectively.

It can be seen from Fig. 11(a) that the strength and initial stiffness of specimen SJ01 are both greater than those of specimen SJ02. The moment resistance of specimen SJ01 is approximately 1.3 times greater than that of SJ02 and the initial stiffness of specimen SJ01 is 1.2 times greater than that of specimen SJ02. After the moment on specimen SJ02 exceeds 33kN.m, a decline on the stiffness of the joint occurs which is due to the overcoming of frictional force between angle and beam flange as shown in Fig. 12. The frictional force between angle and beam flange can be calculated by using the following expression:

$$V = 4\mu F \tag{4}$$

where F stands for the pre-tighten force in one bolt which is 100kN; μ for the friction coefficient which is 0.4 according to the Chinese Code for Design of Steel Structures [23].

The moment resistance of specimen SJ02 referring to the frictional force between angle and beam flange can be expressed as follows:

$$M_f = VH_{beam} \tag{5}$$

where H_{beam} stands for the depth of steel beam which is 0.2m.

According to the above equations, the moment resistance referring to the frictional force is calculated as 32kN.m which is approximately equal to the experimental value. After the frictional force between angle and beam flange has been overcame, the curve of specimen SJ02 goes into a so-called “elastic-plastic” stage in which the discrepancy of the moment resistance between specimen SJ01 and specimen SJ02 becomes larger. In this stage, the connection deformation of specimen SJ02 under bending moment may already involve the out-of-plane deformation of tube wall.

Fig. 11(b) shows the bending moment-tensile force relationship curves of those two specimens. As above mentioned, tensile force was applied on both beam-ends after the specimen yielded. Due to the vertical deformation of the specimen under bending moment, additional moment would be brought to the specimen. Hence, the moment of the specimen in Step B is given as follows:

$$M = P/2 \cdot L - N \cdot \Delta \tag{6}$$

where N stands for the tensile force.

It can be seen from Fig. 11(b) that the bending moment of the specimens is descending along with the increase of tensile force. The relationship of moment resistance and tensile force of specimen SJ01 is nonlinear while that of specimen SJ02 is approximately linear. In this case, the relationship of moment resistance and tensile force of specimen SJ01 could be described by the power function correlation equation derived by fitting with the results of parametric analysis (Gao [24]) as follows:

$$\frac{M}{M_p} + \left(\frac{N}{N_p}\right)^2 = 1 \tag{7}$$

where Mp and Np stand for plastic tensile strength and moment strength of steel beam respectively.

In addition, the behavior of specimen SJ02 under bending moment combined with tensile force could be represented by the linear correlation equation as follows:

$$\frac{M}{M_p} + \frac{N}{N_p} = 1 \tag{8}$$

The correlation equations are validated against the experimental results as shown in Fig. 13. Good agreement is achieved in the comparison of M-N curves. Based on the research in Gao [24], it is worth noticing that the behavior of rigid joint under combined moment and tension could be described by a power function correlation equation, whilst that of semi-rigid joint could be represented by a linear correlation equation. Therefore, the behavior of joint

under combined moment and tension may be uniformly described by the expression as follows:

$$\frac{M}{M_p}+\left(\frac{N}{N_p}\right)^n=1 \tag{9}$$

where *n* stands for the coefficient referring to different types of joint.

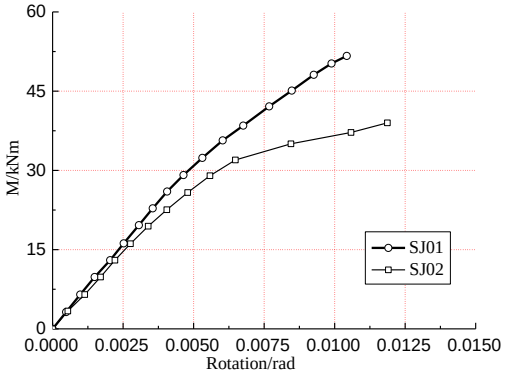

(a) Moment-rotation curves

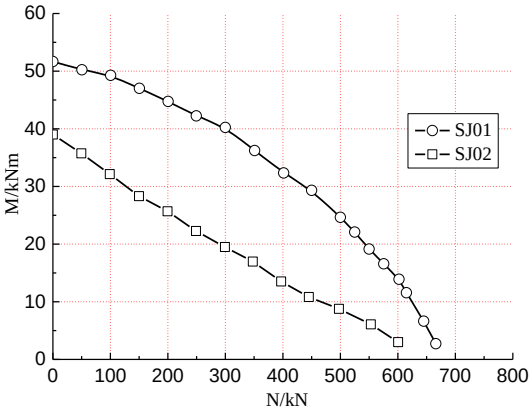

(b) Moment-tensile force curves

Fig. 11 Experimental results

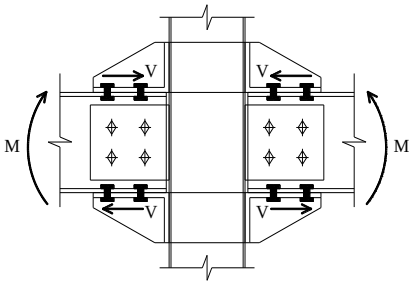

Fig. 12 Frictional froce in specimen SJ02

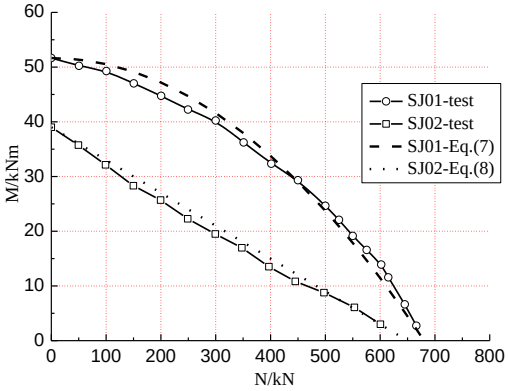

Fig. 13 Comparison of moment-tensile force curves

Fig. 14 shows the horizontal load-vertical displacement relationships in loading Step B. The result of the curves indicates that the vertical displacement of the specimens remains almost constant value with the increase of tensile load. It verifies that the decrease of moment on the specimen is caused by tensile force and the transition of load-carrying mechanism is undergoing from plastic action to catenary action with the increase of tensile force.

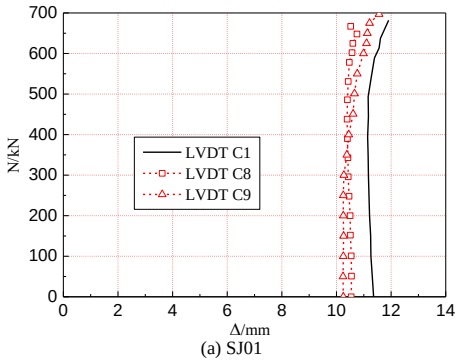

(a) SJ01

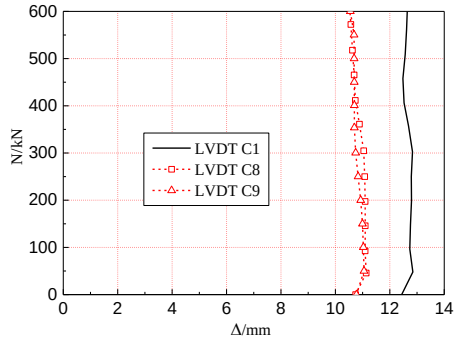

(b) SJ02

Fig. 14 Horizontal load-vertical displacement relationships in loading Step B

4.2. Analysis of strain gauge data

Fig. 15 shows the strains on steel beams in loading Step A. The detailed location of strain gauges can be found in Fig. 8. The vertical lines in Fig. 15 stand for the yield strain of steel which is about 1334 με in this paper. At the early stage of vertical load applied, the section of steel beam is in accordance with plane cross-section assumption and the neutral axis is located in the middle of the section. At 80kN, the strain on the steel beam of specimen SJ01 has reached plastic yield value while the section of the steel beam in SJ02 is still in elastic stage at 60 kN. It indicates that the decrease of moment resistance of specimen SJ02 in Step B is due to the behavior of connection, rather than steel beam itself.

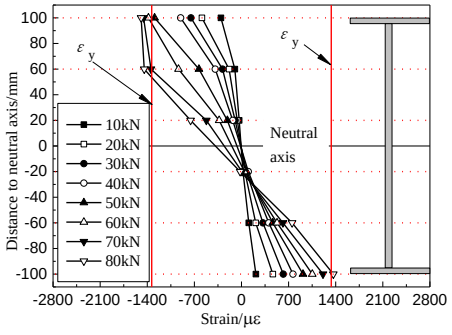

(a) Horizontal load-displacement in Step A (SJ01)

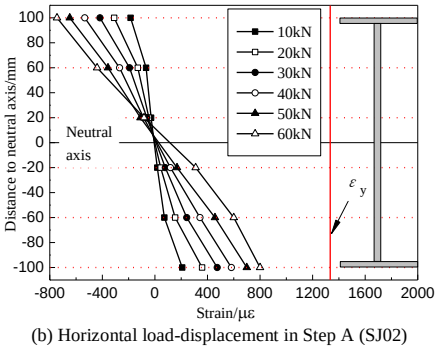

(b) Horizontal load-displacement in Step A (SJ02)

Fig. 15 Strains of steel beam in step A

Fig. 16 shows load-strain relationships in two loading steps. It can be seen from Fig. 16(a-b) that the strain of steel beam increases linearly along with the

increase of vertical load. After tensile loads are applied, the compressive strain of steel beam begins to decrease. At 670 kN, the strain of the whole beam section in specimen SJ01 has reached yield value which means the tensile strength of steel beam has been reached as shown in Fig. 16(c). The test on specimen SJ02 was terminated at 600 kN of tensile load. Even the whole section of steel beam in specimen SJ02 is in tension as shown in Fig. 16(d), part of steel beam has not reached tensile yield strain. It indicates that specimen SJ02 still needs improvement on the mechanical behavior.

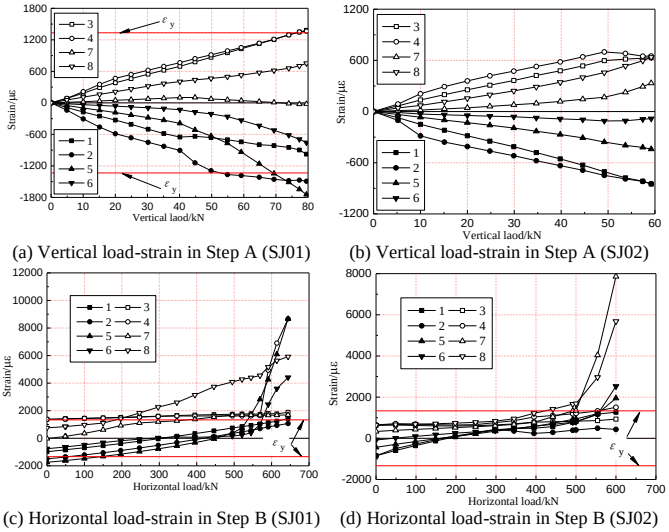

(a) Vertical load-strain in Step A (SJ01) (b) Vertical load-strain in Step A (SJ02)

(c) Horizontal load-strain in Step B (SJ01) (d) Horizontal load-strain in Step B (SJ02)

Fig. 16 Load-strain relationships in two loading steps

5. Numerical analysis

5.1. Finite element modeling and model validation

In addition to study and improve the behavior of the new joint, a finite element model using ABAQUS is developed to validate against the experimental results. Solid elements (C3D8R) are used to simulate the core concrete, steel beam, steel column, angle and bolts. The effects of weld seam and weld residual stress are neglected in the model. The angle components are connected to the tube wall by *Tie command. The bolt preloads are applied as the test by using the command of *Bolt load in ABAQUS. The contact between core concrete and column flange is simulated by "surface to surface interaction" in ABAUQS library. The friction coefficient of 0.3 is adopted in surface tangential friction. Due to the symmetrical arrangement of the specimen and test setup, 1/2 model is employed. The finite element model is shown in Fig. 17.

A bi-linear elastic-plastic material model considering stress hardening from ABAQUS is adopted to model the material properties of steel. The stress-strain relationships of steel member and bolts are identical to those in the material test. The concrete damage plasticity model from ABAQUS library is used to model the concrete material. The stress-strain relationships of concrete material from Chinese code for design of concrete structures (GB50010-2010) as shown in Fig. 18 are introduced into ABAQUS to simulate core concrete. The tensile strength of concrete is defined as 10% compressive strength of concrete. The remaining strength after concrete cracking in tension is 0.5 MPa.

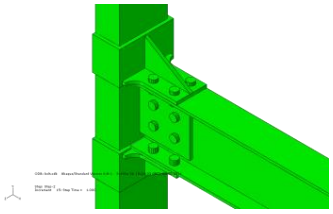

Fig. 17 Finite element model

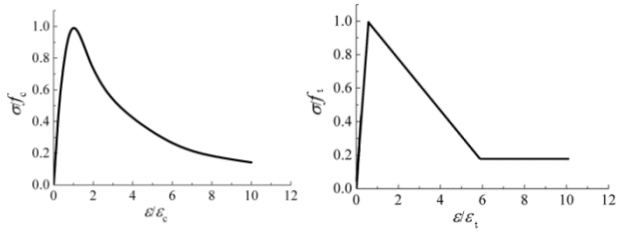

(a) Compressive relationship (b) Tensile relationship

Fig. 18 Stress-strain relationship of concrete

The loading procedure adopted in the simulation is the same as that in the tests. The FE model is validated against the experimental results as shown in Fig. 19. Good agreement is achieved in the simulation of curves. Due to the difficulty in simulation of frictional displacement, a discrepancy occurs after the frictional force has been overcome as shown in Fig. 19(a). The bending moment resistance of the joint descends linearly with the increase of tensional force as shown in Fig. 19(b).

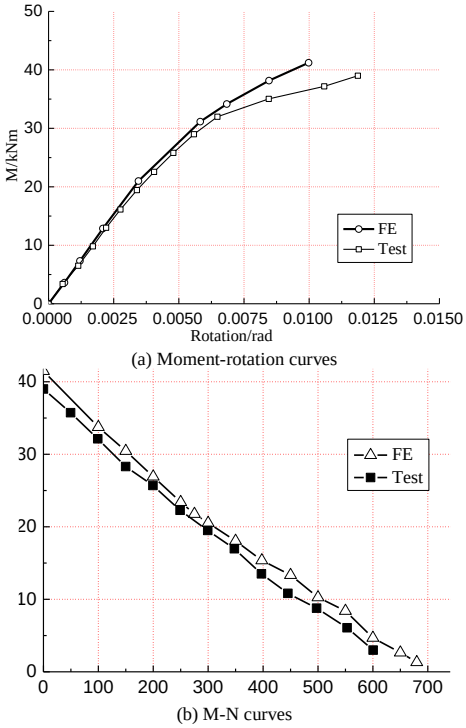

(a) Moment-rotation curves

(b) M-N curves

Fig. 19 Validation of FE model

5.2. Parametric analysis

The configuration of angle has effect on the behavior of new joint. Four parameters of angle profile are analyzed as shown in Fig. 20, namely the short-limb width (bs), short-limb thickness (ts), long-limb width (bl) and long-limb thickness (tl). The cross section of angle in the test was ∟160×100×10 [∟-Long-limb width×Short-limb width×Limb-thickness]. In the study, only one parameter is changed at each group of analysis. The dimensions and materials of the models in parametric analysis are identical to those of the aforementioned FE model.

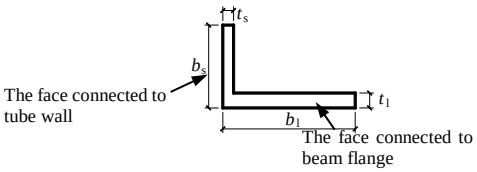

Fig. 20 Unequal-leg angle

Fig. 21 shows the influence of short-limb width from 60 mm to 120 mm on connection properties. Along with the increase of short-limb width, the moment resistance and initial stiffness of the joint both increase. According to the result of stress distribution, the maximum stress occurs at the welding seams between short-limb and tube wall when the short-limb width is 60 mm and 80 mm. When the short-limb width increases to 100mm and 120mm, the maximum stress occurs at the extreme row of bolt hole. In practice, long short-limb is suggested to enhance the behavior of the joint.

Fig. 22 shows the influence of short-limb thickness from 4 mm to 10 mm on connection properties. Along with the decrease of short-limb thickness, the moment resistance and initial stiffness of the joint both decrease. The increase of short-limb thickness would depress the deformation of tube wall. According to the result of stress distribution, the maximum stress occurs at welding seams between short-limb and tube wall when the short-limb thickness is 4 mm and 6 mm. When the short-limb thickness exceeds 8 mm, the maximum stress relocates from the welding seam between short-limb and tube wall to the

extreme row of bolt hole. In the above test, the fracture of welding seams was observed. Therefore particular attention should be paid on the configuration and construction of the welding seam between short-limb and tube wall.

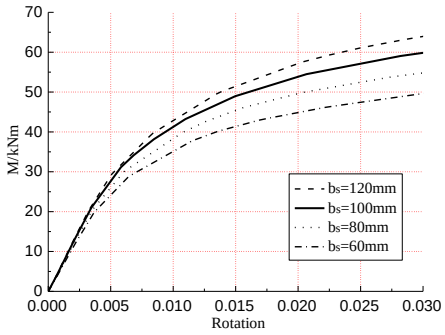

(a) Moment-rotation curves

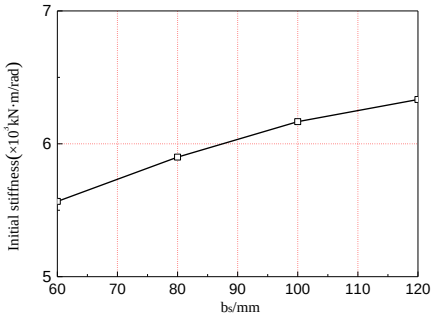

(b) Initial stiffness

Fig. 21 Influence of b_s on connection properties

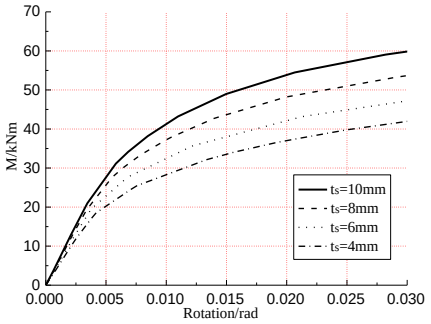

(a) Moment-rotation curves

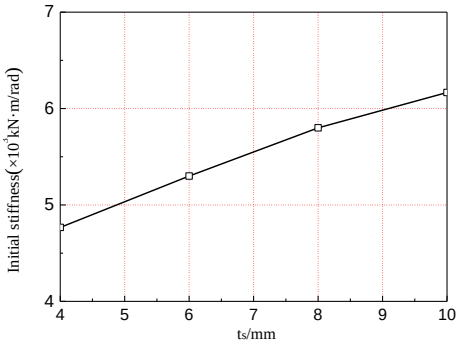

(b) Initial stiffness

Fig. 22 Influence of t_s on connection properties

Fig. 23 shows the influence of long-limb width from 145 mm to 185 mm on connection properties. The long-limb width is increased by extending the bolt-hole spacing whilst the number of bolts remains unchanged. It can be seen from Fig. 23 that the change of long-limb width has little influence on the behavior of the joint.

Fig. 24 shows the influence of long-limb thickness from 6 mm to 12 mm on connection properties. The initial stiffness of the joint increases linearly along with the increase of long-limb thickness. In that case, the shear capacity of bolts group between long-limb and beam flanges would be enhanced by increasing the long-limb thickness. On contrary, the long-limb width shows little influence on the shear capacity of bolts group as described above.

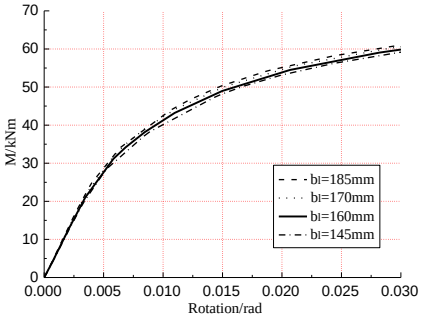

(a) Moment-rotation curves

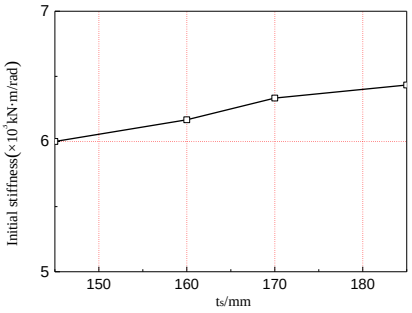

(b) Initial stiffness

Fig. 23 Influence of b_l on connection properties

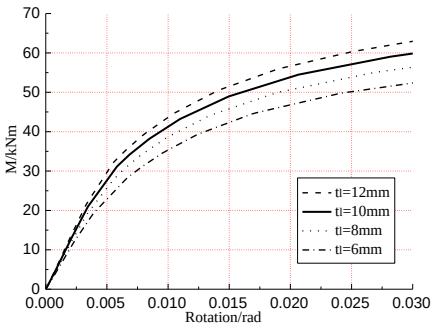

(a) Moment-rotation curves

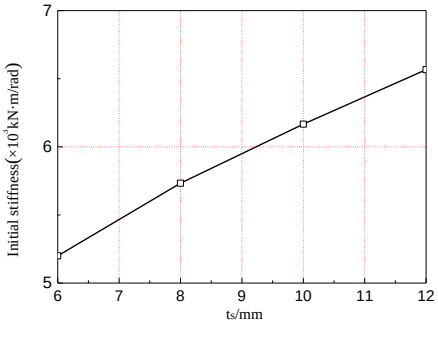

(b) Initial stiffness

Fig. 24 Influence of t_l on connection properties

6. Conclusions

Two CFST column-steel beam joints under bending moment combined with tensile force were tested and studied in detail. In addition, parametric analysis on the new joint was also conducted by using software ABAQUS. Based on the test observations and numerical analysis, the following conclusions are made:

(1). Under pure bending moment, new semi-rigid joint possesses good

rotation capacity. The initial stiffness and moment resistance of the new joint are both smaller than those of rigid joint with outer-ring.

(2). The bending moment capacity of the joints decreases with the increase of tensile force. The bending moment-tensile force relationship of new joint keeps linear. The behavior of rigid and semi-rigid joint under combined moment and tension may be uniformly described by a power function correlation expression.

(3). The numerical analysis result shows that the increase of width of the short-limb connected to tube wall and the limb thickness could enhance the initial stiffness and strength of the new joint whilst the width of the long-limb connected to beam flange shows little influence on the behavior of joint.

Acknowledgments

The research described in this paper was financially supported by National Natural Science Foundation of China (NO. 51408106 and NO. 50878066), Scientific Research Program Funded by Shaanxi Provincial Education Department (17JK1154), Open fund of Shaanxi Key Laboratory of safety and durability of concrete structures (XJKFJJ201803) and Xijing University Special Foundation (XJ17T07) which are gratefully acknowledged.

References

[1] Office of the Deputy Prime Minister, “The Building Regulations 2000, Part A, Schedule 1:A3, Disproportionate Collapse”, London, UK, 2004.
[2] General Services Administration, “Progressive collapse analysis and design guidelines for new federal office buildings and major modernization projects”, Washington (DC), USA, 2003.
[3] Department of Defense, “Unified Facilities Criteria: Design of Building to Resist Progressive Collapse”, New York, USA, 2013.
[4] Haremza C., Satiago A., Demonceau J.F., Jaspart J.P. and Simoes da Silva L., “Composite joints under M-N at elevated tempertures”, Journal of Constructional Steel Research, 124, 173-186, 2016.
[5] Buscemi N. and Marjanishvili S., “SDOF model for progressive collapse analysis”, Proceedings of the 2005 Structures Congress, New York, USA, 2005, April.
[6] Gerasimidis S. and Sideri J., “A new partial-distributed damage method for progressive collapse analysis of steel frames”, Journal of Constructional Steel Research, 119, 233-245, 2016.
[7] Izzuddin B.A., Vlassis A.G., Elghazouli A.Y. and Nethercot D.A., “Progressive collapse of multi-storey buildings due to sudden column loss-Part 1: Simplified assessment framework”, Engineering Structures, 30(5), 1308-1318, 2008.
[8] Iribarren S.B., Berke P., Bouillard Ph., Vantomme J. and Massart T.J., “Investigation of the influence of design and material parameters in the progressive collapse analysis of RC structures”, Engineering Structures, 33, 2805-2820, 2011.
[9] Khandelwal K. and EI-Tawil S., “Collapse behavior of steel special moment resisting frame connections”, Journal of Structural Engineering, 133(5), 646-655, 2007.
[10] Li Y., Lu X.Z., Guan H. and Ye L.P., “An improved tie force method for progressive collapse resistance design of reinforced concrete frame structures”, Engineering Structures, 33, 2931-2942, 2011.
[11] Stylianidis P.M. and Nethercot D.A., “Modelling of connection behaviour for progressive collapse analysis”, Journal of Constructional Steel Research, 113, 169-184, 2015.
[12] Xu G.Q. and Ellingwood B.R., “An energy-based partial pushdown analysis procedure for assessment of disproportionate collapse potential”, Journal of Constructional Steel Research, 67, 547-555, 2011.
[13] Yu X.H., Lu D.G., Qian K. and Li B., “Uncertainty and sensitivity analysis of reinforced concrete frame structures subjected to column loss”, Journal of Performance of Constructed Facilities, No. 04016069, 1-14, 2016.
[14] Yi W.J., He Q.F. and Xiao Y., “Collapse performance of RC frame structure”, Journal of Building Structures, 28(5), 104-117, 2007.
[15] Demonceau J.F. and Jaspart J.P., “Experimental test simulating a column loss in a composite frame”, Advanced Steel Construction, 6, 891-913, 2010.
[16] Sadek F., Main J.A., Lew H.S. and Bao Y.H, “Testing and analysis of steel and concrete beam-column assemblies under a column removal scenario”, Journal of Structural Engineering, 9, 881-892, 2011.
[17] Li L., Wang W., Chen Y.Y. and Lu Y., “Experimental investigation of beam-to-tubular column moment connections under column removal scenario”, Journal of Constructional Steel Research, 88(5), 244-255, 2013.
[18] Yang B., Tan K.Y., Xiong G. and Nie S.D., “Experimental study about composite frames under an internal column-removal scenario”, Journal of Constructional Steel Research, 121, 341-351, 2016.
[19] Qian K., Li B. and Zhang Z.W., “Influence of multicolumn removal on the behavior of RC floors”, Journal of Structural Engineering, 142(5), 04016006, 2016.
[20] Guo L.H., Gao S., Wang Y.Y. and Zhang S.M., “Tests of rigid composite joints subjected to bending moment combined with tension”, Journal of Constructional Steel Research, Vol. 95, 44-55, 2014.
[21] Guo L.H., Gao S. and Fu F., “Structural performance of semi-rigid composite frame under column loss”, Engineering Strucutres, 95, 112-126, 2015.
[22] Hoang V.L., Jaspart J.P., Demonceau J.F., “Extended end-plate to concrete-filled rectangular column joint using long bolts”, Journal of Constructional Steel Research, 113, 156-168, 2015.
[23] Ministry of Construction, “Code for Design of Steel Structures”. Beijing, China, 2003.
[24] Gao S., “Progressive collapse behavior of planar steel frame with composite beam”, Ph.D. Dissertation, Harbin Institute of Technology, Harbin, 2014.